Imaging slab-transported fluids and their deep dehydration from seismic velocity tomography in the Lesser Antilles subduction zone

Lidong Bie [a,b,*], Stephen Hicks [c], Andreas Rietbrock [a], Saskia Goes [c], Jenny Collier [c], Catherine Rychert [d], Nicholas Harmon [d], Benjamin Maunder [c], The VoiLA Consortium [1]

[a] Geophysical Institute (GPI), Karlsruhe Institute of Technology, Germany
[b] School of Environmental Sciences, University of East Anglia, UK
[c] Department of Earth Sciences and Engineering, Imperial College London, UK
[d] Ocean and Earth Science, National Oceanography Centre Southampton, University of Southampton, Southampton, UK

A B S T R A C T

Volatiles play a pivotal role in subduction zone evolution, yet their pathways remain poorly constrained. Studying the Lesser Antilles subduction zone can yield new constraints, where old oceanic lithosphere formed by slow-spreading subducts slowly. Here we use local earthquakes recorded by the temporary VoiLA (Volatile recycling in the Lesser Antilles) deployment of ocean-bottom seismometers in the fore- and back-arc to characterize the 3-D seismic structure of the north-central Lesser Antilles subduction zone. Along the slab top, mapped based on seismicity, we find low Vp extending to 130–150 km depth, deeper than expected for magmatic oceanic crust. The slab's most prominent, elevated Vp/Vs anomalies are beneath the fore- and back-arc offshore Guadeloupe and Dominica, where two subducted fracture zones lie with the obliquely subducting boundary between Proto-Caribbean and Equatorial Atlantic lithosphere. These structures, therefore, enhance hydration of the oceanic lithosphere as it forms and evolves and the subsequent dehydration of mantle serpentinite when subducted. Above the slab, we image the asthenosphere wedge as a high Vp/Vs and moderate Vp feature, indicating slab-dehydrated fluids rising through the overlying cold boundary layer that might induce melting further to the west. Our results provide new evidence for the impact of spatially-variable oceanic plate formation processes on slab dehydration and mantle wedge volatile transfer that ultimately impact volcanic processes at the surface, such as the relatively high magmatic output observed on the north-central islands in the Lesser Antilles.

1. Introduction

The subduction of oceanic plates transports water deep into the Earth mantle. On the way down, approximately half of sediment-carried fluids are expelled at depths of <50 km due to compaction (Rüpke et al., 2004). However, significant volumes of water remain bounded in the descending oceanic crust and mantle in the form of hydrous minerals (e.g., Schmidt and Poli, 1998; van Keken et al., 2011; Garth and Rietbrock, 2014). Particularly, pre-existing fault structures in oceanic lithosphere, such as outer rise normal faults, fracture zones (FZs), and core complex-related detachment faults, may allow deep infiltration of volatiles into the oceanic

mantle (e.g., Manea et al., 2014). When subducted, these hydrous phases break down and release their fluids with increasing pressure and temperature. The first main volatile release pulse comes from the dehydration of oceanic crust, when the slab top reaches the warmer mantle wedge (van Keken et al., 2011). If deep hydration leads to the formation of serpentinite in the slab mantle, its dehydration would generate a second notable volatile release pulse (van Keken et al., 2011), leading to dehydration embrittlement that causes intermediate depth intraslab seismicity (Peacock, 2001; Abers et al., 2006).

Slab dehydration drives the generation of arc and back-arc magmatism through the melting of the overlying mantle wedge. Various fluid migration models are proposed based on seismic imaging, such as vertical, buoyant ascent of fluids (e.g., Harmon and Blackman, 2010), and downward transportation just above the slab (e.g., Tsuji et al., 2008). In the latter model, water expelled from the slab is either bound in a thin layer of hydrous minerals, such as serpentinite/chlorite, or as free fluids in cool, high viscosity and

* Corresponding author at: School of Environmental Sciences, University of East Anglia, UK.
  E-mail address: l.bie@uea.ac.uk (L. Bie).
[1] Details in Appendix A.
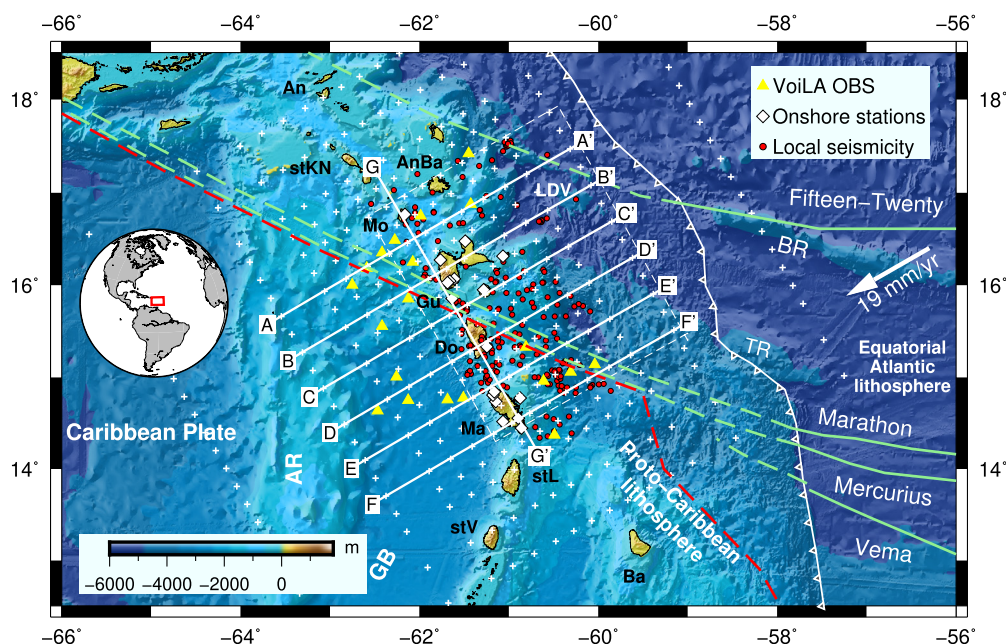
Fig. 1. Map of the north-central section of the Lesser Antilles subduction zone. The inset map shows the location of the study region. VoiLA OBS and onshore seismic stations used in this study are marked by yellow triangles and white diamonds, respectively. Red dots mark earthquakes from Bie et al. (2020) that are used in the tomographic inversions. White crosses show the horizontal grid nodes used in 3-D inversions and white lines are the locations of cross-sections shown in later figures. The area studied by Paulatto et al. (2017) is depicted by dashed white rectangle. Green solid lines indicate the oceanic fractures zones and the continuing dashed lines mark the inferred projection of subducted FZs (Cooper et al., 2020). Red dashed line marks the domain boundary between proto-Caribbean lithosphere and Equatorial Atlantic lithosphere (Braszus et al., 2021). GB, Grenada Basin; AR, Aves Ridge; BR, Barracuda Ridge; TR, Tiburon Rise; LDV, La Désirade Valley; An, Anguilla; AnBa, Antigua & Barbuda; stKN, St. Kitts & Nevis; Mo, Montserrat; Gu, Guadeloupe; Do, Dominica; Ma, Martinique; stL, St. Lucia; stV, St. Vincent; Ba, Barbados. (For interpretation of the colours in the figure(s), the reader is referred to the web version of this article.)

low permeability mantle wedge material just above the subducting plate (Cerpa et al., 2017). Yet, our understanding of water recycling, including volatile delivery and release pathways, amount of water release at various depths, and melt generation in the back-arc wedge, remains incomplete (e.g., Hasegawa, 2018).

By imaging seismic velocities, local earthquake travel-time tomography (LET) is a geophysical tool that can shed light on slab hydration, dehydration, and mantle wedge dynamics. Previous LET studies have primarily centred on fast Pacific subduction zones, such as in Tonga (Zhao et al., 1997), the southern Hikurangi (Eberhart-Phillips et al., 2005), Alaska (Rossi et al., 2006), central America (Syracuse et al., 2008), South America (Hicks et al., 2014), and Mariana (Barklage et al., 2015). They have successfully imaged key domains, such as the subducting slab and mantle wedge, allowing inferences about volatile recycling at various depths. At shallow depths beneath the fore-arc, the slab top is usually imaged as high Vp/Vs, interpreted as over-pressured sediments at the top of hydrated crust and accretionary structures above the slab (e.g., Eberhart-Phillips and Bannister, 2015). In the mantle wedge, hydrous minerals leave a low Vp, high Vp/Vs and high-attenuation signature, consistent with fluid release into the overlying wedge from hydrated oceanic slab (e.g., Wiens et al., 2008; Hasegawa, 2018). If small-volume fluids present in cold, low-permeability mantle immediately above the subducting plate (Cerpa et al., 2017), the mantle wedge may show high Vp/Vs without significantly lowering Vp (Takei, 2002).

A global picture of fluid pathways at subduction zones requires detailed knowledge of Atlantic subduction zones, such as the Lesser Antilles, where old Atlantic lithosphere, formed at a slow-spreading ridge, subducts slowly beneath the Caribbean plate. The Lesser Antilles subduction zone consists of a present-day active arc and an inactive outer arc to the east. Magmatic productivity varies greatly along the arc. Particularly, the central segment (~14°–16° N), including the islands of Guadeloupe, Dominica and

Martinique, has had the highest volume of erupted magma over the last 100,000 years (Wadge, 1984).

Recent seismic and geochemical studies have already revealed a new understanding of volatile recycling, and therefore magmatic productivity variations, for the Lesser Antilles subduction zone. Active source images across the incoming Atlantic lithosphere reveal a highly segmented plate of interspersed magmatically-robust and tectonically-dominated crust prior to subduction (Davy et al., 2020). A thin crust with reduced Vp is observed over a 20–30 km wide zone across the FZ axis. The Marathon FZ shows a lower velocity gradient in the crust than crust at non-transform off-sets, and a sharp increase to mantle velocity at 5.5–6.5 km depth. This strong velocity gradient implies increased fracturing and serpentinization due to larger offset and longer strike-slip faulting activities at the ridge axis. Close to FZs, infiltrated fluids, which facilitate hydrothermal alteration (Hacker et al., 2003), are stored as serpentinized peridotite. It is hypothesised that when subducted, the variations in hydration of the incoming oceanic lithosphere result in along-arc variability in dehydration processes at depth, and hence magmatic output. This process has been recognised by geodynamic numerical simulation (Manea et al., 2014), which revealed the role played by subducted FZs in enhancing production of slab-derived fluids.

Cooper et al. (2020) offer a partial piece of evidence to support the role of subducted FZs by analysing Boron trace elements and isotopic fingerprints of melt inclusions from the Lesser Antilles, which are sensitive to serpentinite. With the seismicity distribution (Bie et al., 2020) and surface-wave derived shear-wave velocities, Cooper et al. (2020) proposed that serpentine-derived fluids from excess mantle hydration along the boundary between older Proto-Caribbean and current Equatorial Atlantic domains, and its coincident FZs (Fig. 1), result in greater mantle wedge melting. The highest concentrations of fluids and melt is below Dominica, which has low Vs in the sub-arc lithosphere (Harmon et al., 2021; Schlaphorst

et al., 2021), and the highest volume of erupted magma of the island arc (Wadge, 1984).

Using local earthquakes recorded by amphibious stations in the fore-arc (Fig. 1), Paulatto et al. (2017) imaged a generally low Vp oceanic crust to depths of 80–100 km and a local low Vp anomaly (<7.5 km/s) at ~50 km depth between Martinique and Montserrat. They proposed that a greater water flux is transported to ~50 km depth by the Marathon FZ compared with other parts of the arc. This study, however, had a maximum imaging depth of 120 km, and therefore lacked resolution west of the arc, and was thus unable to image deeper variations in slab dehydration and the asthenosphere wedge. Teleseismic Rayleigh wave tomography (Harmon et al., 2021) observed low Vs extending 200 km west into the back-arc, which was associated with partial melt or fluids. However, the broad sensitivity of surface waves with 50–100 km lateral resolution cannot resolve deep fluid pathways from the slab to the arc.

The above-mentioned seismic studies and geochemical analysis revealed partially the effect of inherited structures, such as FZs and domain boundary, in delivering fluid. However, the hydration state of the slab and subsequent dehydration processes remain poorly constrained. To what depth does the subducting oceanic crust and mantle transport water? Where does slab mantle dehydration of serpentine occur? Do large-scale oceanic structures facilitate dehydration at greater depth? How do expelled fluids from the slab migrate into the mantle wedge, which could facilitate partial melting? In this study, we use higher resolution seismic velocity imaging with local body waves to probe these questions. We use seismic data from an extensive OBS network covering the fore- and back-arcs (Collier, 2017; Goes et al., 2019) to image the subducting slab and mantle wedge to ~170 km depth. We then use geodynamic models to examine the physical properties of the slab and mantle wedge, and predict where dehydration would occur to interpret the seismic observations. Our results offer new important constraints on deep mantle dehydration, fluid transport and mantle wedge geodynamics for this slow subduction zone.

2. Tectonic background and seismicity

The Lesser Antilles subduction zone in the eastern Caribbean is one of two locations where the Atlantic oceanic lithosphere subducts. The subducting slab consists of material formed at the modern-day Mid-Atlantic ridge ("Equatorial Atlantic" in Fig. 1), and earlier Proto-Caribbean ridge (Cooper et al., 2020). Both ridges were slow-spreading, at a rate of ~20 mm/yr (Müller et al., 2019). The boundary between these two domains tracks obliquely across the study area, currently lying beneath Dominica on the island arc. The lithosphere formed at the proto-Caribbean ridge, up to 120 Myr old, is now fully subducted beneath the southern Lesser Antilles arc. Along most of the arc now, Atlantic lithosphere converges at a rate of ~19 mm/yr (DeMets et al., 2010), and the seafloor at the trench is 80–100 Myr old (Müller et al., 2019; Cooper et al., 2020; Braszus et al., 2021).

The incoming plate displays several major bathymetric structures, including the Barracuda Ridge, Tiburon Rise and FZs (Fig. 1). Several major FZs entering the subduction zone are traceable from the interpretation of the vertical gravity gradient (Braszus et al., 2021). Their projection onto the downgoing slab shows that the Marathon and Mercurius FZs are below the north of Dominica, close to the domain boundary (Harmon et al., 2019; Cooper et al., 2020). To the west of the trench lies the ~300 km wide forearc. A sequence of V-shaped basins is separated by elevated spurs in the northern Lesser Antilles (Boucard et al., 2021), such as the La Désirade Valley offshore Guadeloupe. Below the forearc offshore Dominica-Guadeloupe, Kopp et al. (2011) imaged an 8 km thick oceanic crust of the incoming Atlantic plate.

Seismicity rates are higher for the segment north of Martinique than for the southern arc (e.g., Bie et al., 2020). High b-values were found offshore Martinique (Schlaphorst et al., 2016). Pervasive seismicity beyond 120 km depth below the northern arc suggests deep dehydration of the subducting slab (e.g., Paulatto et al., 2017; Bie et al., 2020). Here, we take advantage of this deep seismicity and shallow earthquakes in the upper plate together with our VoiLA OBS coverage of the back-arc to generate new local Vp and Vp/Vs seismic velocity models. We then compare these models to the water release predicted from thermal models to interpret the deep dehydration processes of the subducting lithosphere, fluid transport, and melt generation in the back-arc.

3. Data and methods

3.1. Data

The VoiLA OBS network, comprising 34 stations, was deployed for 14 months in the fore- and back-arc of the Lesser Antilles subduction zone (Goes et al., 2019). Bie et al. (2020) used this dataset together with recordings from land stations to define a well-constrained 1-D velocity model and obtained 378 well-located events with depth errors less than 1 km, a significant improvement in hypocentral locations compared to those achievable from land-based stations along the island arc alone. Here we use this 1-D relocated earthquake catalogue to generate LET images for the Lesser Antilles subduction zone. Owing to the sparsity of seismicity in the southern arc, along with the strong arc curvature, we limit our analysis to the northern-central part of the Lesser Antilles system, extending from the islands of Antigua in the north to Saint Lucia in the south (Fig. 1). The high-quality subset catalogue includes 235 events with 6,034 P- and 5,145 S-wave arrivals. See Bie et al. (2020) for more details on the travel-time dataset.

### 3.2. Local earthquake travel-time tomography

We use the tomographic inversion package SIMUL2000 (Thurber, 1993; Eberhart-Phillips, 1986; Eberhart-Phillips and Michael, 1998) to determine the Vp and Vp/Vs models. More details on this approach are given in the above papers, along with recent regional-specific studies of Haberland et al. (2009), Collings et al. (2012), Hicks et al. (2014) and León-Ríos et al. (2021). We test a wide range of damping values for the damped least-squares inversion and select the one at the knee of the trade-off curve between data and model variance (Fig. S1). Varying the damping value slightly does not change significantly the tomographic model.

To avoid velocity artefacts for regions with low resolution, we perform a series of inversions with increasing complexity–a "staggered" inversion strategy (e.g., Haberland et al., 2009; Collings et al., 2012; Hicks et al., 2014; León-Ríos et al., 2021). We take the layered 1-D model from Bie et al. (2020) as the initial starting model and invert sequentially for 2-D, arc-perpendicular structure and finally, the 3-D models that allow for along-arc velocity variations. For each step, we first invert for Vp by fixing Vp/Vs, and then we invert for Vp/Vs by fixing the newly-obtained Vp. The previously obtained Vp and Vp/Vs models are used as starting models for the subsequent inversion steps with smaller grid resolution. This strategy ensures that the main 2-D arc perpendicular structure is determined first, and that any unresolved artefacts are not propagated through to the final 3-D model. Final station delays are shown in Fig. S2.

We set the grid spacing so that it is densest near the network centre (Fig. 1) and to maintain roughly a uniform derivative weight sum (DWS) across the grid. We increase the grid spacing away from the arc in both trench-perpendicular, trench-parallel and vertical directions. For the inversions, we set the minimum
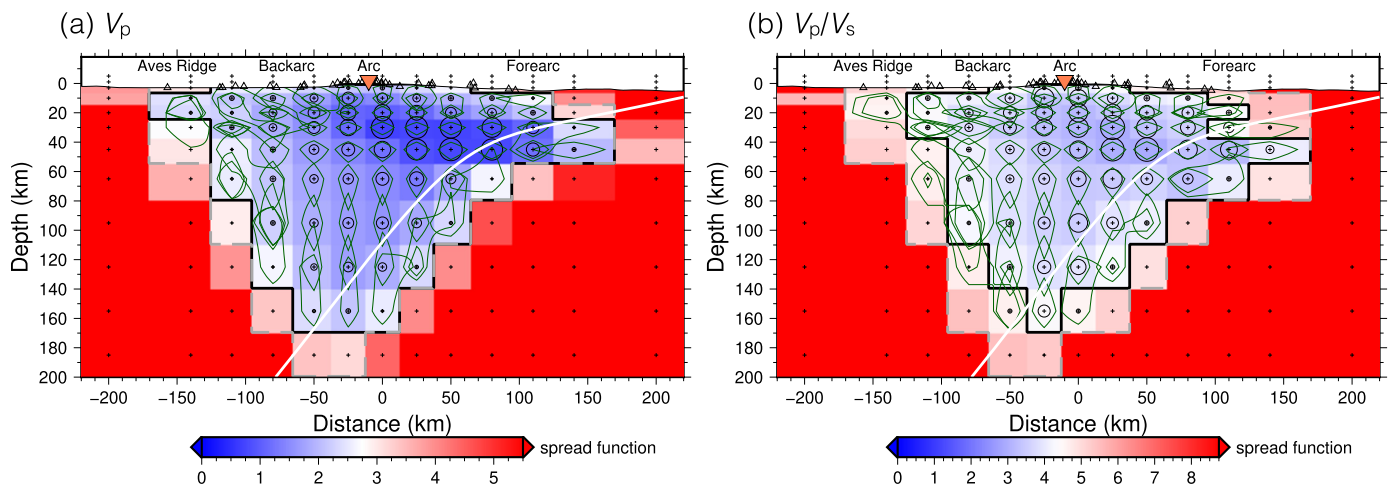
Fig. 2. Resolution estimate for 2-D Vp (a) and Vp/Vs (b) models based on the resolution matrix analysis. The blue-red colours at each node indicate spread function values, black circles represent diagonal elements of the resolution matrix and green lines correspond to the 70% contour of the resolution kernel. Thick black line bounds the regions with good resolution, and dashed grey line bounds less well resolved region. White curved line represents the slab surface defined by the top of the Wadati-Benioff zone seismicity (Bie et al., 2020). Inverted triangle marks the location of island arc. Small black crosses show the velocity inversion nodes.
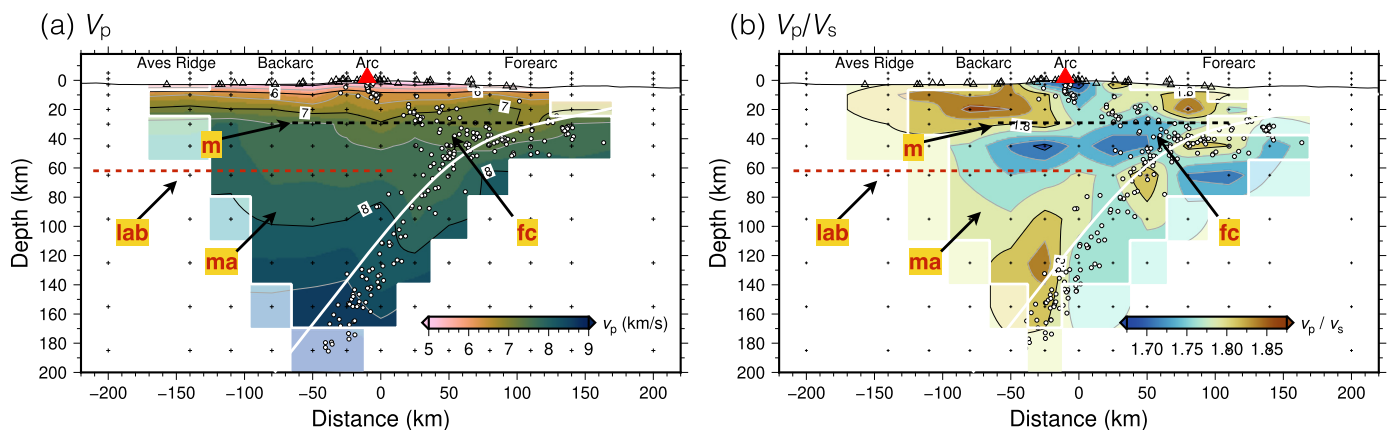
Fig. 3. 2-D velocity models. (a) Vp model. (b) Vp/Vs model. Red dashed line (lab) at ∼60 km depth indicates a velocity decrease from S-to-P receiver functions (Chichester et al., 2019), and black dashed line (m) at ∼30 km depth marks the estimated Moho below the arc from Kopp et al. (2011). Areas with good resolution are bounded by white lines, and areas with reduced resolution are faded, as per Fig. 2. All earthquakes used in the inversion for the 2-D velocity model are projected to the profile. White curved line represents the slab surface across the reference point located at 15°N, 61°W. We note that the slab dip angle changes along the island arc (Bie et al., 2020). Triangles represent seismic stations. Red triangle marks the location of island arc. ma = mantle asthenosphere; fc = forearc corner.

horizontal arc-perpendicular grid spacing at 25 km near the island arc (Fig. 1), and a non-uniform depth spacing based on our input 1-D model (Fig. 2 in Bie et al., 2020). In the 3-D inversion, an along-arc grid spacing of 25 km is used (Fig. 1). Our carefully designed grid spacing ensures a good ray path coverage of the areas where most seismicity and stations are located (Fig. S3). Fig. 2 shows the resolution estimate for 2-D Vp and Vp/Vs models based on the resolution matrix analysis, detailed in Appendix B with additional model resolution tests.

4. Results and interpretation of main structural domains

We now outline the key features in the obtained velocity models, describing first the main 2-D structure, followed by along-arc variations imaged by the 3-D inversion. Fig. 3 shows our new 2-D model perpendicular to the arc. The 3-D model is shown in cross-sections perpendicular to (Fig. 4), and along the arc (Fig. 5), and in map views at 20, 65, 95 and 120 km depth (Fig. S4).

4.1. 2-D velocity models

The 2-D velocity model illustrates the first-order features across the north-central Lesser Antilles subduction zone (Fig. 3). Beneath

the arc, the 7 km/s contour extends to 30 km depth, compared to ∼20 km depth in the back- and fore-arc regions. It likely reflects thicker sub-arc crust. There is also a markedly lower Vp/Vs in the arc crust (∼1.70) compared to the fore- and back-arc (>1.80).

At 30–60 km depth below the fore-arc, arc and back-arc, Vp is 7.3–7.8 km/s, and the Vp/Vs is between 1.70 and 1.75 (Fig. 3). The 7.75 km/s contour in Fig. 3 aligns well with a velocity decrease imaged by S-to-P receiver functions at ∼60 km depth (Chichester et al., 2019). This boundary was interpreted as the transition from lithosphere to melt-bearing asthenosphere. We similarly interpret this ∼30 km thick layer as the lithospheric mantle of the Caribbean plate. The fore-arc corner (fc in Fig. 3) of the upper plate, which comprises seismic activity, has a low-to-moderate Vp/Vs (1.70–1.75) and moderate Vp (7.2–7.7 km/s).

The dipping velocity contours that coincide with seismicity demarcate the westerly-dipping slab (Fig. 3). The slab top has a lower Vp than the overlying mantle wedge and underlying subducting plate. This feature coincides with an elevated Vp/Vs (>1.80) down to ∼80 km depth. At 80–140 km depth, the Vp/Vs of the slab top is moderate (∼1.75), but increases again (>1.80) below 140 km depth.
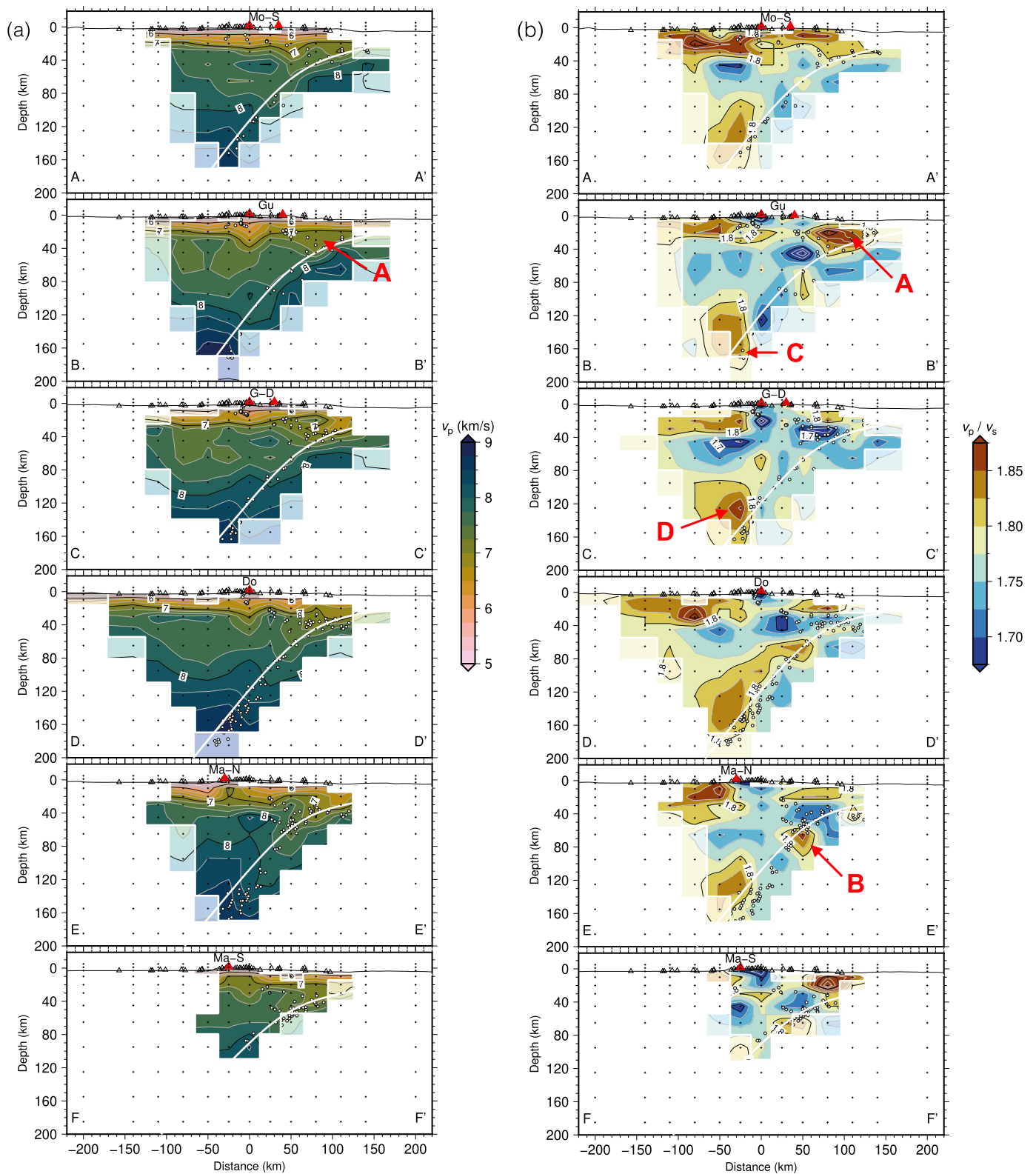
Fig. 4. Arc-perpendicular profiles through the final 3-D Vp (a) and Vp/Vs (b) models. Profile locations are in Fig. 1. White circles show seismicity within 25 km of each profile. Anomalies labelled "A", "B", "C" and "D" are discussed in the text. Red triangle marks the location of island arc; where two triangles are presented, the west one is present-day active arc and the other is inactive outer arc to the east. Mo-S, Montserrat-South; Gu, Guadeloupe; G-D, between Guadeloupe and Dominica; Do, Dominica; Ma-N, Martinique-North; Ma-S, Martinique-South.

In the back-arc, the most prominent feature shown in the 2-D model is the high Vp/Vs (>1.78) mantle wedge beneath 80 km depth, in an area where Vp is moderate to high, increasing from 7.8 km/s at 80 km depth to 8.7 km/s at 160 km depth. This high

Vp/Vs extends into the slab, and the highest Vp/Vs value is above the slab at 120–130 km depth, and ~15 km west of the arc.

Given the potential significance of the Vp/Vs features in the back-arc mantle, we devised a restoring resolution test to inves-
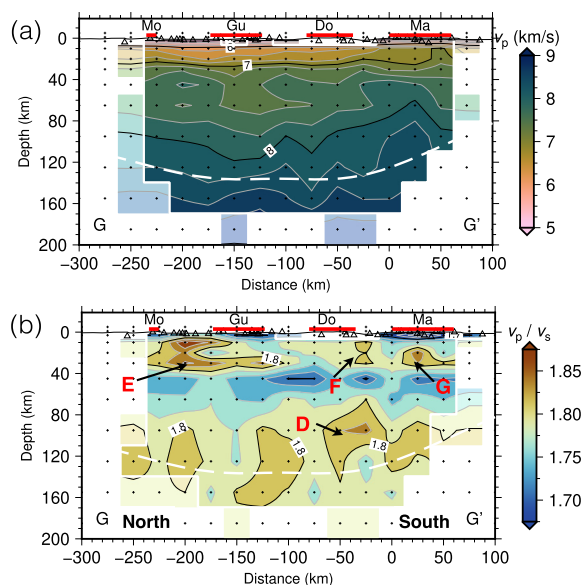
Fig. 5. Cross section G–G' along the arc. Profile locations are in Fig. 1. White dashed line shows the intersection of the cross section and the slab surface. Red bands on top of each figure show the lateral extent of individual islands as labelled. Anomalies labelled "D", "E", "F" and "G" are discussed in the text.

tigate how well they are resolved. We generated a synthetic travel time dataset by designing velocity models that consider abstract features from the 2-D imaged velocity anomalies (Fig. 3b) and conducted forward modelling based on the given source-receiver geometry. Particularly, we designed an elevated Vp/Vs anomaly in the back-arc that penetrates through the slab surface (Fig. 6a). A low Vp/Vs is assigned to the lithospheric mantle with a sharp difference to the above and below regions (Fig. 6a). As shown in the recovered model (Fig. 6b), the input low and high Vp/Vs anomalies are well recovered. However, the low Vp/Vs feature representing the lithospheric mantle of the Caribbean plate smears vertically with the high Vp/Vs below in the wedge. Smearing is also observed in the NW and SE directions of this low Vp/Vs anomaly, consistent with that suggested by resolution matrix and checkerboard tests (Appendix B). The deep high Vp/Vs anomaly is reproduced at its input location, but with slightly reduced maximum amplitude from 1.85 to 1.83. Two additional 2-D tests suggest that the high Vp/Vs features both above and within the slab beneath 80 km depth are required by the data and represent true physical features (Fig. S5).

4.2. 3-D velocity models

Overall, the 3-D velocity models (Figs. 4 and 5) show consistent large-scale features from the 2-D cross sections. The 3-D models also highlight important variations along the arc.

The shallowest velocity contours indicate crustal thickness variations in the region. For instance, the 7.25 km/s contour line extends to 45 km depth beneath Guadeloupe and 30 km depth beneath Martinique, likely reflecting thicker crust beneath Guadeloupe (Fig. 4a and 5a). The back-arc has a ubiquitously high Vp/Vs at depths <30 km, and the high Vp/Vs forearc crust is particularly pronounced ~40 km east of Guadeloupe, corresponding to a reduced Vp of 7.2 km/s (anomaly "A" in profile B–B' of Fig. 4a and b).

The velocity structure of the lithospheric mantle of the overlying Caribbean plate varies along the arc. Several profiles contain areas of higher Vp lithosphere below the forearc (in particular D–D', E–E' and F–F'). In all profiles, the upper plate contains large areas of reduced Vp (7.5–7.75 km/s) and moderate to low Vp/Vs

between 1.70 and 1.75 at 40–60 km depth, particularly below the back-arc.

All profiles suggest that the slab is lower in Vp than the overlying plate/mantle and deeper part of the slab (Fig. 4a). The 7.5 km/s contour along the slab, often interpreted to demarcate the transition from the basaltic slab crust to eclogite, extends to 40–60 km depth. Most of the slab is characterised by relatively low Vp/Vs, but a high Vp/Vs region is present at the slab top in all cross-sections at 60–90 km depth, reaching 15 km into the slab. At this depth, the slab beneath Martinique has the highest Vp/Vs value (>1.85) (anomaly "B" in profile E–E' of Fig. 4b), compared to lower Vp/Vs (1.80–1.85) further north.

Below 120 km depth, a high Vp/Vs anomaly (>1.80) is present in all cross-sections from Montserrat in the north to Martinique in the south (Fig. 4b), and the highest value is seen beneath Guadeloupe (anomaly "C" in profile B–B' of Fig. 4b). In all cases, this anomaly extends into the mantle wedge. The highest Vp/Vs (>1.85) in the asthenospheric wedge lies ~25 km west of Dominica (anomaly "D" in profile C–C' of Fig. 4b).

To further illustrate the along-strike variations of the mantle wedge and subducting slab, Fig. 5 shows our 3D model on an along-arc section. As described above, the depths of the velocity contours at shallow depths vary beneath the four islands, likely reflecting variations in crustal thickness, consistent with those found by Melekhova et al. (2019). High Vp/Vs is present in the sub-arc crust with values of 1.78–1.85. At 40–60 km depth, the lowest Vp/Vs is found between Guadeloupe and Dominica in the lithospheric mantle. Beneath 60 km depth, high Vp/Vs (>1.78) dominates, with several locally increased but disconnected areas as depicted by the Vp/Vs = 1.80 contour. The slab top aligns with the 8.25 km/s Vp contour, and there are punctuated regions of elevated Vp/Vs (>1.80) above and below the slab top.
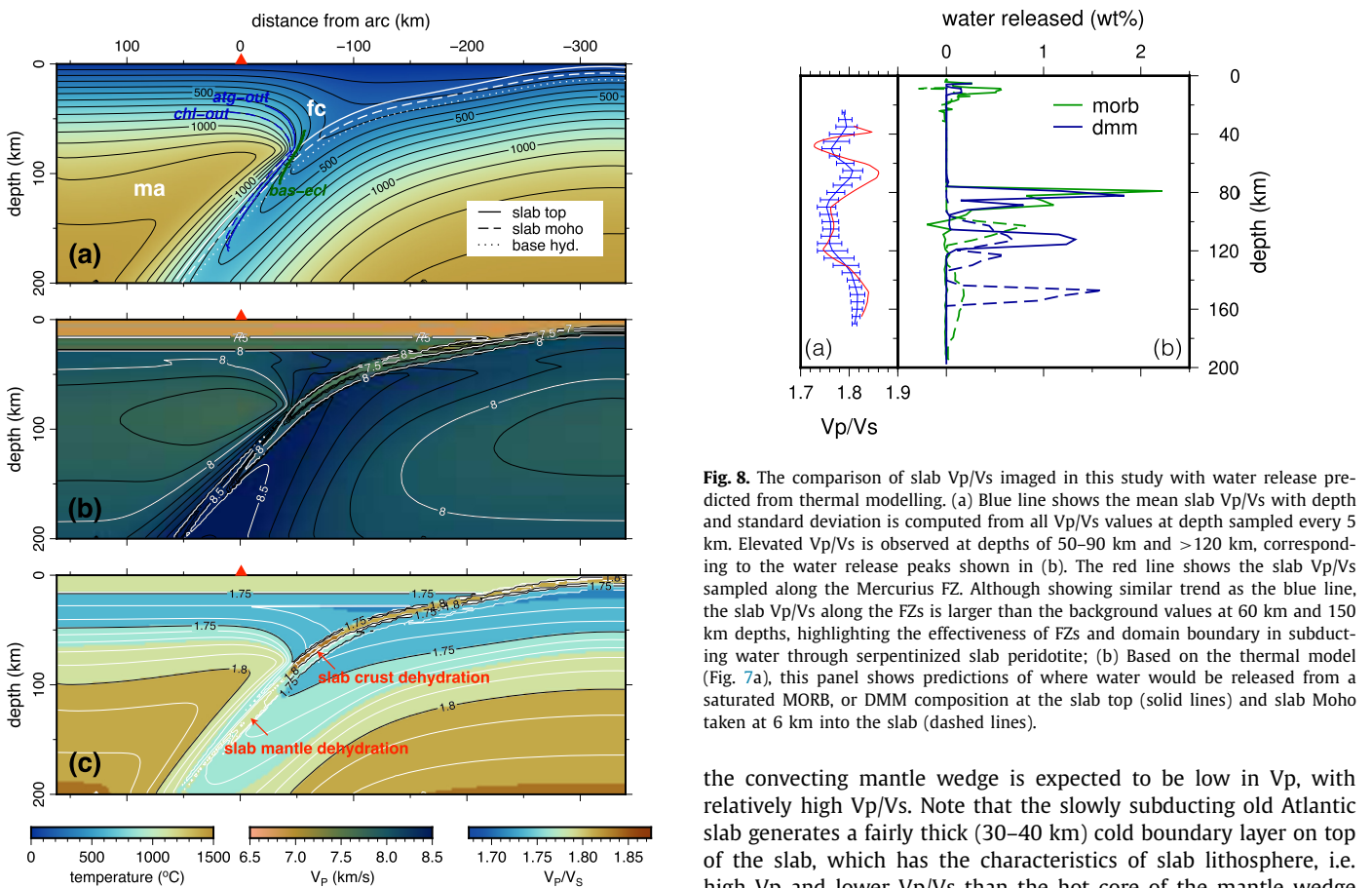
5. Thermal and synthetic seismic velocity structure

To assist with interpreting the slab, wedge and upper plate mantle-lithosphere velocities, we ran a kinematic thermal model (Fig. 7a) to predict seismic velocities that would result from variations in temperature, pressure and mineralogy. Our model set-up is similar to Perrin et al. (2018) and Halpaap et al. (2019), and its specific application to the Lesser Antilles is described by Harmon et al. (2021). Additional details of thermal dynamic modelling setup are in Appendix B.

Our modelling predicts relatively low Vp and high Vp/Vs in the hydrated basaltic slab crust (Fig. 7b and c). The blueschist to eclogite transition occurs where the slab is first exposed to warm convecting mantle material at the coupling transition depth (CTD) at 80 km depth and is accompanied by dehydration and a substantial increase in Vp and decrease in Vp/Vs. The hydrated layer of harzburgite contributes to the low velocities at the top of the slab and persists to at least 160 km depth. Fig. 8b shows where water is released from a saturated mid-ocean ridge basalt (MORB), or depleted MORB-source mantle (DMM) composition at the slab top and slab Moho. Mafic crust would generate the most prominent fluid release signatures near the CTD. Serpentinised mantle in the upper part of the slab would also generate a signature around the CTD yet would yield additional deeper high Vp/Vs where antigorite and chlorite break down, around depths of 110 km (if at the slab top) and 150 km (if present 6 km into the slab). The depth extents of these Vp/Vs anomalies associated with slab fluids are visible in Fig. 8b. Our synthetic models do not include the signature of free fluids but do predict where dehydration of different mineralogies (hydrous magmatic crust or lithospheric mantle) would occur. Near the depths where peaks in dehydration occur, we would expect an additional reduced Vp and especially elevated Vp/Vs in the mantle wedge overlying the slab top.
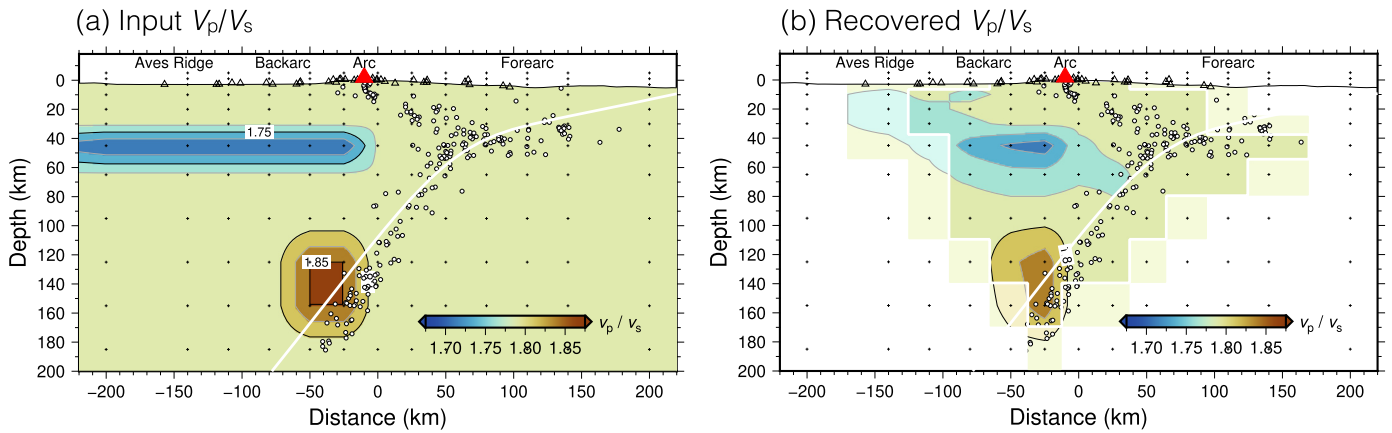
Fig. 6. Restoring resolution test for 2-D Vp/Vs. (a) Input Vp/Vs model including a high Vp/Vs mantle wedge in and above the slab from 110 to 170 km depth, and low Vp/Vs anomaly at 40–60 km depth in the back-arc. (b) Recovered Vp/Vs model showing that the deep anomaly in the back-arc is well-recovered, whereas the shallow low Vp/Vs anomaly is smeared between 80 km depth and the surface.

Fig. 7. 2-D synthetic thermal and seismic velocity structure along a cross section through Dominica in the direction of plate motion. Details of the modelling procedure are described in Harmon et al. (2021). (a) Thermal structure from a kinematically driven model (plate geometry from Bie et al., 2020; subducting plate velocity of 2 cm/yr; upper plate cooling age of 60 Myr and coupling transition depth of 80 km) superimposed by the main dehydration boundaries (basalt to eclogite ("bas-ecl") transition in MORB/gabbro, and antigorite-out ("atg-out") and chlorite-out ("chl-out") boundaries in DMM/harzburgite). (b) Vp (c) Vp/Vs computed assuming dry DMM composition for the mantle and most of the mantle lithosphere, MORB crust at the top 6 km of the subducting plate, hydrous harzburgite (2.5 wt% water) for 6 km below the MORB crust (base labelled as "base hyd."). Red triangle marks the location of island arc. ma = mantle asthenosphere; fc = forearc corner.

Our synthetic model shows that the upper-plate lithosphere is expected to be relatively high in Vp and low in Vp/Vs. In contrast,
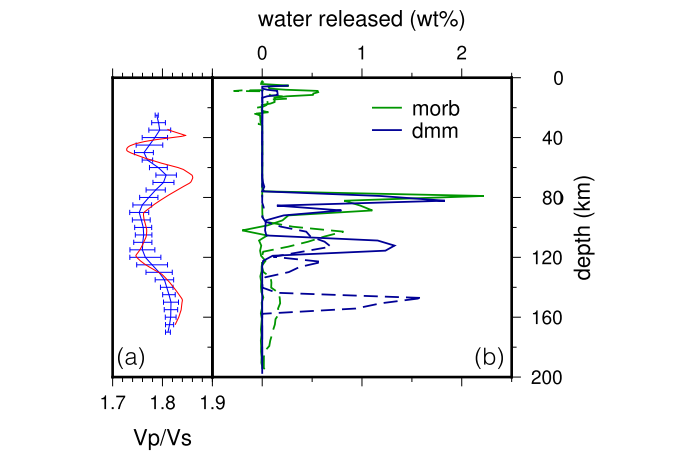

Fig. 8. The comparison of slab Vp/Vs imaged in this study with water release predicted from thermal modelling. (a) Blue line shows the mean slab Vp/Vs with depth and standard deviation is computed from all Vp/Vs values at depth sampled every 5 km. Elevated Vp/Vs is observed at depths of 50–90 km and >120 km, corresponding to the water release peaks shown in (b). The red line shows the slab Vp/Vs sampled along the Mercurius FZ. Although showing similar trend as the blue line, the slab Vp/Vs along the FZs is larger than the background values at 60 km and 150 km depths, highlighting the effectiveness of FZs and domain boundary in subducting water through serpentinized slab peridotite; (b) Based on the thermal model (Fig. 7a), this panel shows predictions of where water would be released from a saturated MORB, or DMM composition at the slab top (solid lines) and slab Moho taken at 6 km into the slab (dashed lines).

the convecting mantle wedge is expected to be low in Vp, with relatively high Vp/Vs. Note that the slowly subducting old Atlantic slab generates a fairly thick (30–40 km) cold boundary layer on top of the slab, which has the characteristics of slab lithosphere, i.e. high Vp and lower Vp/Vs than the hot core of the mantle wedge (Fig. 7b-c).

6. Implications for volatile cycling

6.1. Fore-arc fluids and melt in the sub-arc crust

One prominent feature in the overriding Caribbean crust is the reduced Vp (7.2 km/s) and high Vp/Vs reaching 1.88 in the inner fore-arc about 40 km to the east of the volcanic arc. This anomaly is largest and strongest offshore Guadeloupe (the anomaly "A" in profile B–B' of Fig. 4). This feature extends to the slab interface (the anomaly "A" in Fig. 9). Paulatto et al. (2017) found a similar Vp/Vs anomaly in this location. They interpreted it as the result of thick sediment packages underthrust and transported on the slab
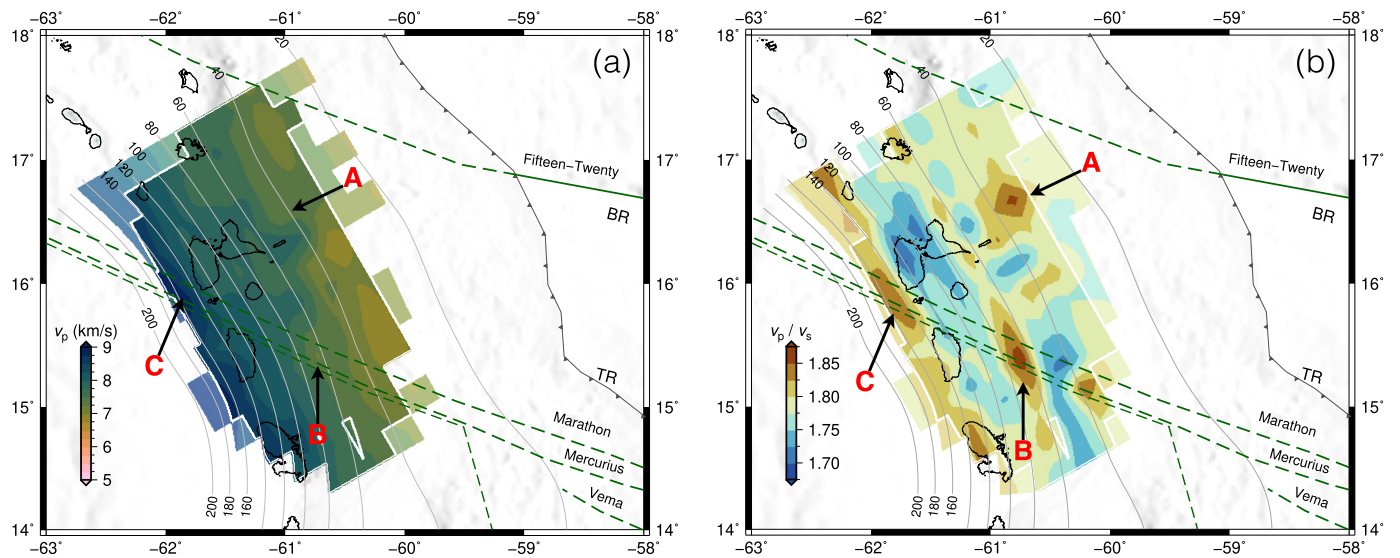
Fig. 9. Vp (a) and Vp/Vs (b) along the slab interface. The values within 5 km of the slab surface (Bie et al., 2020) are averaged and shown here. Green lines depict FZs and domain boundary as shown in Fig. 1. Depth to the top of the slab is shown by the grey contours.

top with the Tiburon Rise and Barracuda ridge. This high Vp/Vs and reduced Vp feature correlates at the seafloor with the La Désirade Valley, the largest of several V-shaped basins separated by elevated spurs in the northern Lesser Antilles (Boucard et al., 2021). We interpret the anomaly as an imprint of saturated sediments deposited in La Désirade Valley. Our resolution limits mean that we cannot rule out a contributing effect from thick subduction sediments along the plate interface that extends deeper than 40 km (Laigle et al., 2013).

In the forearc and back-arc upper crust, generally higher Vp/Vs values (>1.75) at crustal depths (<30 km) are suggestive of extensive fluid saturation. Fluid infiltration into crustal fractures and a substantial diffuse upward water flux (Paulatto et al., 2017) could generate a water-rich upper crust that can explain such high Vp/Vs. By contrast, much of the volcanic arc has a lower Vp/Vs (<1.73) in the upper crust and high Vp/Vs (>1.78) in the lower crust (Fig. 5b). This pattern of low Vp/Vs in the upper crust and high Vp/Vs in the lower crust, also imaged by Paulatto et al. (2017), is consistent with partial melt in the lower crust. Although the Vp/Vs is high (>1.78), it does not exceed 1.85, in agreement with previous receiver function results (Arnaiz-Rodríguez et al., 2016). Melekhova et al. (2019) estimated Vp/Vs under the condition that melts wet grain boundaries completely and thus are fully interconnected for anhydrous basaltic melt in an olivine matrix. They predicted high Vp/Vs of 2.01 for 5 vol% of fully interconnected melt. Our study reports a Vp/Vs range of 1.78–1.85 for the lower crust, much lower than the estimated high Vp/Vs for fully interconnected melt. These high Vp/Vs anomalies in the upper and lower crust occur separately between Montserrat and Guadeloupe (the anomaly "E" in Fig. 5b), between Dominica and Martinique (the anomaly "F" in Fig. 5b), and beneath Martinique (the anomaly "G" in Fig. 5b). Therefore, our result favours the existence of isolated partial melt pockets instead of pervasively distributed partial melt that may supply the active volcanic arc. Another interesting feature in the crustal high Vp/Vs anomalies is two connected high Vp/Vs cores at different depths, such as the ones beneath Montserrat and Dominica. Whether this vertically-connected feature indicates connected magma storage zones, and how this reconciles with volcanic processes need to be further investigated with petrological constraints.

In the shallow forearc mantle corner (marked as fc in Fig. 3; Fig. 4), Vp is relatively low at 7.5–7.8 km/s, but faster than the overlying crust, and Vp/Vs is moderate at 1.75–1.78. These charac-

teristics are consistent with localised and low-degree serpentinization of the mantle peridotite. We estimate up to ~10% serpentinite content in the forearc mantle corner, and corresponding water contents of up to ~2% (Carlson and Miller, 2003). Limited slab dehydration below the fore-arc is consistent with subduction of old and hence cold Atlantic lithosphere (Abers et al., 2017). The fore-arc corner is also characterised by seismicity between ~30–60 km depth above the slab (Figs. 3 and 4). Temperatures here are below those where serpentinite would break down (Fig. 7a). Thus, these events are likely due to shallow fluid release from the subducting slab/sediments, which may trigger earthquakes (e.g., Laigle et al., 2013; Halpaap et al., 2019).

6.2. Subducting slab dehydration

The down-going oceanic crust is imaged with low Vp that follows the Wadati-Benioff seismicity down to ~150 km (Fig. 3a), with its greatest depth beneath northern Martinique (Fig. 4a). We can identify localised anomalies with high Vp/Vs at the slab top along the down-going slab, one at ~30–40 km depth and the other at ~55–80 km depth (Fig. 3b and 4b). The one at shallow depth likely corresponds to the release of free fluids stored in the slab crust and overlying sediments, leading to high pore fluid pressure directly above the slab top. The feature at ~55–80 km depth co-incides with the high Vp/Vs in the crust predicted just above the basalt/eclogite transition (Fig. 7) and subsequent dehydration peak (Fig. 8b), releasing fluids in the overlying wedge corner, where the free fluids would lower Vp/Vs. In both cross-sections along the slab (Fig. 9b) and map view (Fig. S4b), an elongated arc-parallel region of high Vp/Vs is visible at ~55–80 km depth, corresponding to the peak of averaged Vp/Vs at this depth range (Fig. 8a). This observation suggests the accumulation of over-pressured pore fluids on the plate interface due to the main dehydration pulse of both hydrous crust and/or exhumed mantle-lithosphere near CDT (Fig. 7 and Fig. 8). We note that this elongated high Vp/Vs feature at ~55–80 km depth varies along the arc; the lowest Vp and highest Vp/Vs of 1.86 lies offshore Dominica and Martinique (anomaly "B" in Fig. 9), much greater than the averaged along-arc Vp/Vs of ~1.80 at 65 km depth (Fig. 8a). The variability indicates a substantial variation in the degree of hydration. Fig. 9 shows that the local anomaly "B" overlaps with the projection of the domain boundary/Marathon and Mercurius FZs. The co-location indicates that increased fracturing near FZs allows deeper and more pervasive
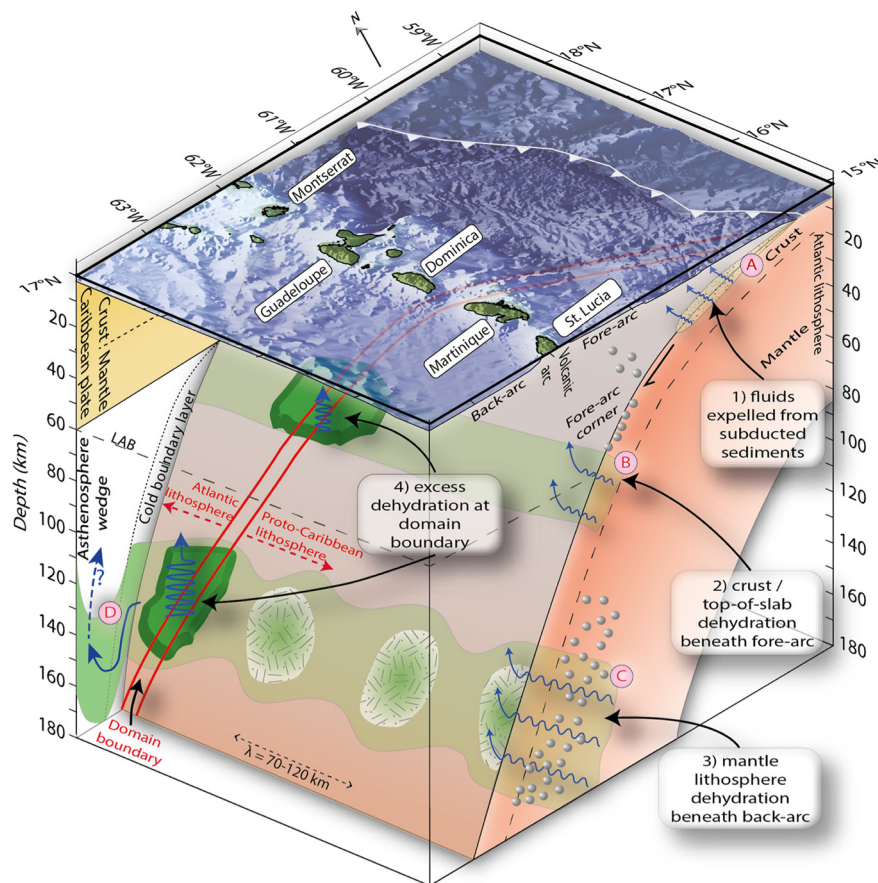
Fig. 10. Schematic interpretation showing down-dip and along-arc variations in structures, fluid transport, and slab dehydration in the Lesser Antilles subduction zone based on findings in this study. Shaded green areas represent the main zones of slab dehydration. Red circles approximately represent the main cluster of seismicity. Red lines mark the inferred projection of subducted FZs (Cooper et al., 2020), and the domain boundary between proto-Caribbean lithosphere and Equatorial Atlantic lithosphere (Braszus et al., 2021).

fluid infiltration into the slab mantle, probably leading to greater peridotite serpentinization that is particularly efficient at incorporating water (up to 14 wt% at saturation in a harzburgite compared to ∼6 wt% for a saturated MORB, Hacker, 2008).

Beyond ∼95 km depth, Vp increases gradually with depth along the slab top, from 7.9 km/s to 8.7 km/s at 170 km depth, where our resolution diminishes (Fig. 3a). Moderate Vp/Vs (1.75–1.78) is found between the depth of 90–120 km along the slab top and increases to >1.80 beneath 120 km, where it extends into the slab mantle (Fig. 3b, 4b and 9b). At the top of the slab, the persistence of a low-velocity layer, relative to the mantle above and slab mantle below, down to 150–170 km depth, and the high Vp/Vs below 120 km depth are consistent with dehydration of serpentinized mantle (Fig. 4). Substantial serpentinisation is compatible with tectonized slab lithosphere, as imaged on the incoming Atlantic lithosphere (Davy et al., 2020). At 130 km depth, the upper mantle of the slab has a temperature of over 500 °C (Fig. 7a; van Keken et al., 2011), allowing dehydration of serpentinite, leading to the second major water release peak from DMM at ∼140 km depth (Fig. 8). Abundant seismicity occurs within the slab (Fig. 3b), with a thick Wadati-Benioff zone of 40 km (Bie et al., 2020) extending to 180 km depth beneath Dominica and Martinique. This seismicity is consistent with a mechanism of dehydration embrittlement. There is significant along-strike variability in the high Vp/Vs anomaly strength in the deep slab. The peak Vp/Vs of 1.84 in the deep slab (anomaly "C" in Fig. 9b) coincides with the subducted domain boundary/Marathon and Mercurius FZs west of Guadeloupe. Our finding highlights increased slab hydration along the domain boundary at even greater depths than the ∼65 km anomaly de-

scribed above. Our interpretation of enhanced hydration via serpentinized mantle peridotite is also consistent with boron isotope signatures in magmas from Guadeloupe and Dominica (Cooper et al., 2020).

6.3. Fluid flux in the asthenosphere mantle wedge beneath the back-arc

The slab crust and lithospheric mantle fluids released below the CTD will ascend and flux into the asthenospheric mantle wedge above the slab. At the top of the subducted slab, the back-arc mantle shows elevated Vp/Vs (>1.78) up to 60 km depth (Figs. 3b and 4b). This feature extends at least 70 km west of the arc, where our resolution diminishes. Although the elevated Vp/Vs is found all along-strike in the back-arc mantle wedge, amplitudes of the Vp/Vs anomalies vary along the arc. The highest Vp/Vs (∼1.85) appears west of northern Dominica (the anomaly "D" in Figs. 4b and 5b). In cross-section D–D' through Dominica (Figs. 4b), this deep (80–160 km) back-arc high Vp/Vs connects on its up-dip side with the high Vp/Vs anomaly on top of the slab at 60–80 km depth, forming the spatially largest high Vp/Vs anomaly in our study. In addition, a series of high Vp/Vs pockets (as delineated by the Vp/Vs = 1.80 contour beneath 80 km depth below the arc) extend into the slab (Fig. 5b). These anomalies appear to repeat with a wavelength of 70–120 km (Fig. 10). This along-arc heterogeneity, even just for the ∼300 km long north-central segment that this study covers, suggests substantial variations in the volume of water released from the subducting slab. This variation is consistent with Davy et al. (2020), who found heterogeneous hydration in the incoming plate. The most prominent high Vp/Vs anomaly beneath

Dominica may highlight a rich fluid source that once fluxed into the warmer parts of the wedge, that is consistent with the peak in magmatic output along the entire volcanic arc (Wadge, 1984) and geochemical signatures (Cooper et al., 2020). Therefore, our tomographic images support the notion that variable hydration of the incoming plate governs volcanic output.

A remaining question thus surrounds the generation of melt in the mantle wedge and how it is transported to the volcanic arc. Whether the high Vp/Vs in the back-arc mantle wedge represents fluids or partial melt depends on mantle temperature and whether it exceeds the solidus. As shown by the modelled thermal structure in this study, the temperature of the mantle wedge within 50 km above the slab is <1350 °C (Fig. 7a). The slow subduction of old, and hence cold Atlantic lithosphere results in such a relatively thick and cool boundary layer on top of the subducting slab. Such a cold boundary layer (Fig. 10) could plausibly have low permeability (Cerpa et al., 2017). The presence of fluids in this layer may lead to high Vp/Vs without significantly lowering Vp (Takei, 2002) as we have imaged. Further to the west in the back-arc, increasing temperatures may promote partial melt, as evidenced by low Vs extending up to 200 km west (Harmon et al., 2021), and a high attenuation anomaly that is laterally offset west of the arc by 50–70 km (Hicks et al., 2019).

High Vp/Vs should therefore be observed further to the west in the back-arc mantle wedge for partial melting. We note that Vp/Vs is reasonably high (>1.75) 70 km west of the arc. Our restoring test (Fig. 4) shows that the Vp/Vs below 65 km depth in the back-arc is affected by the smearing effect from the above Caribbean lithospheric mantle which has Vp/Vs smaller than 1.75. So, the wedge Vp/Vs is likely high ubiquitously below the back-arc imaged here. Combining our inference of fluids in the cold layer directly above the slab, our tomographic results suggest a curved, instead of vertical, fluid migration pathway from slab to arc. Fluids are first dragged down to greater depth with the down-going slab before rising through the warmer back-arc asthenosphere wedge (Fig. 10). Such a model is supported by the geodynamic study of Cerpa et al. (2017). We speculate that the strongest partial melting of the hydrated asthenospheric mantle occurs further to the west in the back-arc. Further constraints on the melt and its pathways to surface beneath the Lesser Antilles arc will be offered by future studies of seismic attenuation (e.g., Hicks et al., 2019).

7. Conclusions

This paper presents a detailed 3-D Vp velocity and Vp/Vs model across the north-central Lesser Antilles island arc down to ∼170 km depth. Fig. 10 summarises our key interpretations described as follows. The velocity model shows a west-dipping slab with decreased Vp to ∼150 km depth. On the slab top, there are three high Vp/Vs anomalies. The shallow one at ∼30–40 km depth represents hydrated slab crust and high pore fluid pressure, where the fluid source is likely related to subducted sediment. The second anomaly at 55–80 km depth may indicate the presence of enhanced serpentinite dehydration in the slab crust along the subducted Marathon and Mercurius FZs and a boundary between the proto-Caribbean domain and the current Equatorial Atlantic domain. Thirdly, elevated Vp/Vs on the slab interface at ∼130 km depth west of Guadeloupe and Dominica coincides with the same domain boundary. This high Vp/Vs in the slab, together with a thick Wadati-Benioff zone >130 km depth, suggests deep dehydration of the slab mantle. Our results highlight the role played by inherited oceanic tectonic structures in transporting fluids down into the mantle and their output along volcanic arcs. In the back-arc, immediately above the slab, the mantle wedge is moderate in Vp and high in Vp/Vs, indicative of free fluids from slab mantle dehydration migrating into the overlying cold boundary layer.

The strongest partial melting of the hydrated asthenospheric mantle may occur further to the west, tentatively indicating a curved fluid migration pathway from slab to the volcanic arc at the surface, where we infer isolated partial melt in the lower crust.

CRediT authorship contribution statement

Lidong Bie: Conceptualization, Methodology, Investigation, Formal Analysis, Visualization, Writing – original draft, Writing – review & editing. **Stephen Hicks:** Conceptualization, Methodology, Investigation, Formal Analysis, Writing – review & editing. **Andreas Rietbrock:** Conceptualization, Methodology, Formal Analysis, Writing – review & editing, Funding acquisition. **Saskia Goes:** Conceptualization, Investigation, Formal Analysis, Writing – review & editing, Funding acquisition. **Jenny Collier:** Conceptualization, Writing – review & editing, Funding acquisition. **Catherine Rychert:** Conceptualization, Writing – review & editing, Funding acquisition. **Nick Harmon:** Conceptualization, Writing – review & editing, Funding acquisition. **Benjamin Maunder:** Investigation, Formal Analysis. **The VoiLA Consortium:** Conceptualization, Writing – review & editing, Funding acquisition. All authors participated in the geophysical experiment to collect seismic data used in this study.

Declaration of competing interest

The authors declare that they have no known competing financial interests or personal relationships that could have appeared to influence the work reported in this paper.

Appendix A. Supplementary material

Supplementary material related to this article can be found online at https://doi.org/10.1016/j.epsl.2022.117535.

References

Abers, G.A., van Keken, P.E., Kneller, E.A., Ferris, A., Stachnik, J.C., 2006. The thermal structure of subduction zones constrained by seismic imaging: implications for slab dehydration and wedge flow. Earth Planet. Sci. Lett. 241 (3–4), 387–397. https://doi.org/10.1016/j.epsl.2005.11.055.

Abers, G.A., Van Keken, P.E., Hacker, B.R., 2017. The cold and relatively dry nature of mantle forearcs in subduction zones. Nat. Geosci. 10 (5), 333–337. https://doi.org/10.1038/NGEO2922.

Arnaiz-Rodríguez, M.S., Schmitz, M., Audemard, F., 2016. La estructura cortical del arco de las Antillas Menores estimada a partir de la técnica de funciones receptoras. Rev. Mex. Cienc. Geol. 33, 286–296.

Barklage, M., Wiens, D.A., Conder, J.A., Pozgay, S., Shiobara, H., Sugioka, H., 2015. P and S velocity tomography of the Mariana subduction system from a combined land-sea seismic deployment. Geochem. Geophys. Geosyst. 16 (3), 681–704. https://doi.org/10.1002/2014GC005627.

Bie, L., Rietbrock, A., Hicks, S., Allen, R., Blundy, J., Clouard, V., et al., 2020. Along-arc heterogeneity in local seismicity across the Lesser Antilles subduction zone from a dense ocean-bottom seismometer network. Seismol. Res. Lett. 91 (1), 237–247. https://doi.org/10.1785/0220190147.

Boucard, M., Marcaillou, B., Lebrun, J.-F., Laurencin, M., Klingelhoefer, F., Laigle, M., et al., 2021. Paleogene V-shaped basins and Neogene subsidence of the Northern Lesser Antilles forearc. Tectonics 40, e2020TC006524. https://doi.org/10.1029/2020TC006524.

Braszus, B., Goes, S., Allen, R., Rietbrock, A., Collier, J., Harmon, N., et al., 2021. Subduction history of the Caribbean from upper-mantle seismic imaging and plate reconstruction. Nat. Commun. 12, 4211. https://doi.org/10.1038/s41467-021-24413-0.

Carlson, R.L., Miller, D.J., 2003. Mantle wedge water contents estimated from seismic velocities in partially serpentinized peridotites. Geophys. Res. Lett. 30 (5), 1250. https://doi.org/10.1029/2002GL016600.

Cerpa, N.G., Wada, I., Wilson, C.R., 2017. Fluid migration in the mantle wedge: influence of mineral grain size and mantle compaction. J. Geophys. Res., Solid Earth 122 (8), 6247–6268. https://doi.org/10.1002/2017JB014046.

Chichester, B., Rychert, C., Harmon, N., Collier, J., Henstock, T., Goes, S.D.B., et al., 2019. Seismic Imaging of the Lesser Antilles Subduction Zone Using S-to-P Receiver Functions. AGU Fall Meeting Abstracts, vol. 53. Retrieved from http://adsabs.harvard.edu/abs/2019AGUFM.S53C0521C.

Collier, J.S., 2017. VoiLA - Volatile recycling in the Lesser Antilles arc: RRS James Cook cruise report JC149. https://www.bodc.ac.uk/resources/inventories/cruise_inventory/reports/jc149.pdf. 161.

Collings, R., Lange, D., Rietbrock, A., Tilmann, F., Natawidjaja, D., Suwargadi, B., et al., 2012. Structure and seismogenic properties of the Mentawai segment of the Sumatra subduction zone revealed by local earthquake travel time tomography. J. Geophys. Res., Solid Earth 117, B01312. https://doi.org/10.1029/2011JB008469.

Cooper, G.F., Macpherson, C.G., Blundy, J.D., Maunder, B., Allen, R.W., Goes, S., et al., 2020. Variable water input controls evolution of the Lesser Antilles volcanic arc. Nature 582 (7813), 525–529. https://doi.org/10.1038/s41586-020-2407-5.

Davy, R.G., Collier, J.S., Henstock, T.J., the VoiLA consortium, 2020. Wide-angle seismic imaging of two modes of crustal accretion in mature Atlantic Ocean crust. J. Geophys. Res., Solid Earth 125 (6), e2019JB019100. https://doi.org/10.1029/2019JB019100.

DeMets, C., Gordon, R.G., Argus, D.F., 2010. Geologically current plate motions. Geophys. J. Int. 181, 1–80. https://doi.org/10.1111/j.1365-246X.2009.04491.x.

Eberhart-Phillips, D., 1986. Three-dimensional velocity structure in northern California Coast Ranges from inversion of local earthquake arrival times. Bull. Seismol. Soc. Am. 76 (4), 1025–1052.

Eberhart-Phillips, D., Michael, A.J., 1998. Seismotectonics of the Loma Prieta, California, region determined from three-dimensional Vp, Vp/Vs, and seismicity. J. Geophys. Res. 103, 21,099–21,120. https://doi.org/10.1029/98JB01984.

Eberhart-Phillips, D., Reyners, M., Chadwick, M., Chiu, J.M., 2005. Crustal heterogeneity and subduction processes: 3-D Vp, Vp/Vs and Q in the southern North Island, New Zealand. Geophys. J. Int. 162 (1), 270–288. https://doi.org/10.1111/j.1365-246X.2005.02530.x.

Eberhart-Phillips, D., Bannister, S., 2015. 3-D imaging of the northern Hikurangi subduction zone, New Zealand: variations in subducted sediment, slab fluids and slow slip. Geophys. J. Int. 201 (2), 838–855. https://doi.org/10.1093/gji/ggv057.

Garth, T., Rietbrock, A., 2014. Downdip velocity changes in subducted oceanic crust beneath Northern Japan – insights from guided waves. Geophys. J. Int. 198 (3), 1342–1358. https://doi.org/10.1093/gji/ggu206.

Goes, S., Collier, J., Blundy, J., Davidson, J., Harmon, N., Henstock, T., et al., 2019. Project VoiLA: volatile recycling in the Lesser Antilles. Eos Trans. AGU 100. https://doi.org/10.1029/2019EO117309.

Haberland, C., Rietbrock, A., Lange, D., Bataille, K., Dahm, T., 2009. Structure of the seismogenic zone of the southcentral Chilean margin revealed by local earthquake travel time tomography. J. Geophys. Res., Solid Earth 114, B01317. https://doi.org/10.1029/2008jb005802.v.

Hacker, B.R., 2008. H$_2$O subduction beyond arcs. Geochem. Geophys. Geosyst. 9 (3). https://doi.org/10.1029/2007GC001707.

Hacker, B.R., Abers, G.A., Peacock, S.M., 2003. Subduction factory 1. Theoretical mineralogy, densities, seismic wave speeds, and H$_2$O contents. J. Geophys. Res., Solid Earth 108 (B1). https://doi.org/10.1029/2001JB001127.

Halpaap, F., Rondenay, S., Perrin, A., Goes, S., Ottemöller, L., Austrheim, H., et al., 2019. Earthquakes track subduction fluids from slab source to mantle wedge sink. Sci. Adv. 5 (4). https://doi.org/10.1126/sciadv.aav7369.

Harmon, N., Blackman, D.K., 2010. Effects of plate boundary geometry and kinematics on mantle melting beneath the back-arc spreading centers along the Lau Basin. Earth Planet. Sci. Lett. 298 (3–4), 334–346. https://doi.org/10.1016/j.epsl.2010.08.004.

Harmon, N., Rychert, C., Collier, J., Henstock, T., van Hunen, J., Wilkinson, J., 2019. Mapping geologic features onto subducted slabs. Geophys. J. Int. 219 (2), 725–733. https://doi.org/10.1093/gji/ggz290.

Harmon, N., Rychert, C.A., Goes, S., Maunder, B., Collier, J., Henstock, T., et al., 2021. Widespread hydration of the back arc and the link to variable hydration of the incoming plate in the Lesser Antilles from Rayleigh wave imaging. Geochem. Geophys. Geosyst. 22, e2021GC009707. https://doi.org/10.1029/2021GC009707.

Hasegawa, A., 2018. Seismic imaging of mantle wedge corner flow and arc magmatism. Proc. Jpn. Acad. Ser. B 94 (5), 217–234. https://doi.org/10.2183/pjab.94.015.

Hicks, S.P., Rietbrock, A., Ryder, I.M., Lee, C.S., Miller, M., 2014. Anatomy of a megathrust: the 2010 M8.8 Maule, Chile earthquake rupture zone imaged using seismic tomography. Earth Planet. Sci. Lett. 405, 142–155. https://doi.org/10.1016/j.epsl.2014.08.028.

Hicks, S.P., Maunder, B.L., Bie, L., Rychert, C., Harmon, N., Goes, S.D., Rietbrock, A., 2019. Evidence for an anomalously large cold Mantle wedge corner of the Caribbean Plate in the Lesser Antilles subduction zone. In: AGU Fall Meeting 2019, T23A-08.

Kopp, H., Weinzierl, W., Becel, A., Charvis, P., Evain, M., Flueh, E.R., et al., 2011. Deep structure of the central Lesser Antilles Island Arc: relevance for the formation of continental crust. Earth Planet. Sci. Lett. 304 (1–2), 121–134. https://doi.org/10.1016/j.epsl.2011.01.024.

Laigle, M., Hirn, A., Sapin, M., Bécel, A., Charvis, P., Flueh, E., et al., 2013. Seismic structure and activity of the north-central Lesser Antilles subduction zone from an integrated approach: similarities with the Tohoku forearc. Tectonophysics 603, 1–20. https://doi.org/10.1016/j.tecto.2013.05.043.

León-Ríos, S., Bie, L., Agurto-Detzel, H., Rietbrock, A., Galve, A., Alvarado, A., et al., 2021. 3D local earthquake tomography of the Ecuadorian margin in the source area of the 2016 Mw7.8 Pedernales earthquake. J. Geophys. Res., Solid Earth 126, e2020JB020701. https://doi.org/10.1029/2020JB020701.

Manea, V.C., Leeman, W.P., Gerya, T., Manea, M., Zhu, G., 2014. Subduction of fracture zones controls mantle melting and geochemical signature above slabs. Nat. Commun. 5 (1), 1–10. https://doi.org/10.1038/ncomms6095.

Melekhova, E., Schlaphorst, D., Blundy, J., Kendall, J.M., Connolly, C., McCarthy, A., Arculus, R., 2019. Lateral variation in crustal structure along the Lesser Antilles arc from petrology of crustal xenoliths and seismic receiver functions. Earth Planet. Sci. Lett. 516, 12–24. https://doi.org/10.1016/j.epsl.2019.03.030.

Müller, R.D., Zahirovic, S., Williams, S.E., Cannon, J., Seton, M., Bower, D.J., et al., 2019. A global plate model including lithospheric deformation along major rifts and orogens since the Triassic. Tectonics 38 (6), 1884–1907. https://doi.org/10.1029/2018TC005462.

Paulatto, M., Laigle, M., Galve, A., Charvis, P., Sapin, M., Bayrakci, G., et al., 2017. Dehydration of subducting slow-spread oceanic lithosphere in the Lesser Antilles. Nat. Commun. 8 (1), 1–11. https://doi.org/10.1038/ncomms15980.

Peacock, S.M., 2001. Are the lower planes of double seismic zones caused by serpentine dehydration in subducting oceanic mantle? Geology 29 (4), 299–302. https://doi.org/10.1130/0091-7613(2001)029<0299:ATLPOD>2.0.CO;2.

Perrin, A., Goes, S., Prytulak, J., Rondenay, S., Davies, D.R., 2018. Mantle wedge temperatures and their potential relation to volcanic arc location. Earth Planet. Sci. Lett. 501, 67–77. https://doi.org/10.1016/j.epsl.2018.08.011.

Rossi, G., Abers, G.A., Rondenay, S., Christensen, D.H., 2006. Unusual mantle Poisson's ratio, subduction, and crustal structure in central Alaska. J. Geophys. Res., Solid Earth 111 (B9). https://doi.org/10.1029/2005JB003956.

Rüpke, L.H., Morgan, J.P., Hort, M., Connolly, J.A., 2004. Serpentine and the subduction zone water cycle. Earth Planet. Sci. Lett. 223 (1–2), 17–34. https://doi.org/10.1016/j.epsl.2004.04.018.

Schlaphorst, D., Kendall, J.M., Collier, J.S., Verdon, J.P., Blundy, J., Baptie, B., et al., 2016. Water, oceanic FZs and the lubrication of subducting plate boundaries—insights from seismicity. Geophys. J. Int. 204 (3), 1405–1420. https://doi.org/10.1093/gji/ggv509.

Schlaphorst, D., Harmon, N., Kendall, J.M., Rychert, C.A., Collier, J., Rietbrock, A., Goes, S., VoiLA Team, 2021. Variation in upper plate crustal and lithospheric mantle structure in the greater and Lesser Antilles from ambient noise tomography. Geochem. Geophys. Geosyst. 22 (7), e2021GC009800. https://doi.org/10.1029/2021GC009800.

Schmidt, M.W., Poli, S., 1998. Experimentally based water budgets for dehydrating slabs and consequences for arc magma generation. Earth Planet. Sci. Lett. 163 (1–4), 361–379. https://doi.org/10.1016/S0012-821X(98)00142-3.

Syracuse, E.M., Abers, G.A., Fischer, K., MacKenzie, L., Rychert, C., Protti, M., et al., 2008. Seismic tomography and earthquake locations in the Nicaraguan and Costa Rican upper mantle. Geochem. Geophys. Geosyst. 9 (7). https://doi.org/10.1029/2008GC001963.

Takei, Y., 2002. Effect of pore geometry on Vp/Vs: from equilibrium geometry to crack. J. Geophys. Res., Solid Earth 107 (B2), 2043. https://doi.org/10.1029/2001JB000522.

Thurber, C.H., 1993. Local earthquake tomography: velocities and Vp/Vs–theory. In: Iyer, H.M., Hirahara, K. (Eds.), Seismic Tomography: Theory and Practice. Chapman and Hall, London, pp. 563–583.

Tsuji, Y., Nakajima, J., Hasegawa, A., 2008. Tomographic evidence for hydrated oceanic crust of the Pacific slab beneath northeastern Japan: implications for water transportation in subduction zones. Geophys. Res. Lett. 35, L14308. https://doi.org/10.1029/2008GL034461.

van Keken, P.E., Hacker, B.R., Syracuse, E.M., Abers, G.A., 2011. Subduction factory: 4. Depth-dependent flux of H$_2$O from subducting slabs worldwide. J. Geophys. Res., Solid Earth 116 (B1). https://doi.org/10.1029/2010JB007922.

Wadge, G., 1984. Comparison of volcanic production rates and subduction rates in the Lesser Antilles and Central America. Geology 12 (9), 555–558.

Wiens, D.A., Conder, J.A., Faul, U.H., 2008. The seismic structure and dynamics of the mantle wedge. Annu. Rev. Earth Planet. Sci. 36, 421–455. https://doi.org/10.1146/annurev.earth.33.092203.122633.

Zhao, Dapeng, Xu, Yingbiao, Wiens, Douglas A., Dorman, LeRoy, Hildebrand, John, Webb, Spahr, 1997. Depth extent of the Lau back-arc spreading center and its relation to subduction processes. Science 278 (5336), 254–257. https://doi.org/10.1126/science.278.5336.254.